

Mapping the Chemo-dynamics of the Galactic disk using the LAMOST and APOGEE red clump stars

Weixiang Sun^{1,3}, Han Shen², Biwei Jiang^{1,3}, and Xiaowei Liu^{2,3}

Submitted to ApJS; Accepted March 03, 2024

ABSTRACT

A detailed measurement is made of the metallicity distributions, kinematics and dynamics of the thin and thick disks, across a large disk volume ($5.0 \leq R \leq 15.0$ kpc and $|Z| \leq 3.0$ kpc), by using the LAMOST-APOGEE red clump stars. The metallicity distributions results show that the radial metallicity gradient $\Delta[\text{Fe}/\text{H}]/\Delta R$ of the thin disk weakens with $|Z|$ from -0.06 dex kpc^{-1} at around $|Z| < 0.25$ kpc to -0.02 dex kpc^{-1} at around $|Z| > 2.75$ kpc, while the thick disk displays a global weak positive $\Delta[\text{Fe}/\text{H}]/\Delta R$, generally weaker than 0.01 dex kpc^{-1} . The vertical metallicity gradient $\Delta[\text{Fe}/\text{H}]/\Delta|Z|$ weakened steadily from -0.36 dex kpc^{-1} at $R \sim 5.5$ kpc to -0.05 dex kpc^{-1} at around $R > 11.5$ kpc for the thin disk, while the thick disk presents an almost constant value (nearly $-0.06 \sim -0.08$ dex kpc^{-1}) for all the R bins. These results indicate the contribution of the radial migration to the disk evolution, and the obvious north-south asymmetry in $[\text{Fe}/\text{H}]$ may be linked to the disk warp and/or the disk perturbation events. The oscillations of the corrected $\Delta[\text{Fe}/\text{H}]/\Delta|Z|$ with R are likely because of the resonances with the Galactic Bar. Our detailed measurements of $\Delta V_{\phi}/\Delta[\text{Fe}/\text{H}]$ indicate an “inside-out” and “upside-down” star formation scenario for the thick disk. The results of eccentricity distributions and $[\alpha/\text{Fe}]$ -velocity dispersion relations are likely to suggest that the thick disk stars require an obvious contribution from other heating mechanisms such as merger and accretion, or born in the chaotic mergers of gas-rich systems and/or turbulent interstellar medium.

Keywords: Stars: abundance – Stars: kinematics and dynamics – Galaxy: disk – Galaxy: formation and evolution

1. INTRODUCTION

Exploring the nature of the Galactic disk plays an important role in understanding the formation and evolution of the disk galaxies (e.g., Yoshii 1982; Hartkopf & Yoss 1982; Bensby et al. 2005; Pilkington et al. 2012; Kordopatis et al. 2015; Gaia Collaboration et al. 2023a,b). Since the first discovered the thin and thick disks of the Milky Way by fitting the vertical stellar density profile with two exponential functions (e.g., Yoshii 1982; Gilmore & Reid 1983), the idea of working on two independent disk components of the Galaxy has become the most mainstream and constructive idea in Galactic archaeology.

The thin and thick disks are not only different in spatial structure (e.g., Du et al. 2003; Bensby et al. 2005; Chang et al. 2011), but also in chemistry, age and kinematics, as well as chemo-dynamics (e.g., Fuhrmann 1998; Lee et al. 2011; Bland-Hawthorn & Gerhard 2016; Miranda et al. 2016; Mackereth et al. 2017; Sun et al. 2020, 2023).

Spatially, the scale-heights of thin and thick disks are about $0.2 \sim 0.4$ kpc and $0.6 \sim 1.0$ kpc (e.g., Du et al. 2006; Jurić et al. 2008; Bland-Hawthorn & Gerhard 2016), respectively. The scale-lengths of thin and thick disks are about $1.0 \sim 4.7$ kpc and $2.0 \sim 5.5$ kpc (e.g., Bilir et al. 2006; Karaali et al. 2007; Jia et al. 2014; Mackereth et al. 2017), respectively.

Regards to chemistry and age, the thin disk stars generally have richer metallicity ($[\text{Fe}/\text{H}]$), lower α -abundance ratio ($[\alpha/\text{Fe}]$), and younger ages than those of the thick disk stars (e.g., Fuhrmann 2008; Haywood et al. 2013; Vickers et al. 2021; Gent et al. 2022; Lian et al. 2022), with the $[\text{Fe}/\text{H}]$ dis-

tribution function of thin and thick disks respectively peaking around -0.2 dex and $-0.5 \sim -0.6$ dex (e.g., Wyse & Gilmore 1995; Soubiran, Bienaymé & Siebert 2003; Kordopatis et al. 2011; Hayden et al. 2015; Sun et al. 2020), and the $[\alpha/\text{Fe}]$ is lower by $0.2 \sim 0.3$ dex for the thin disk stars than that for the thick disk stars (e.g., Lee et al. 2011; Adibekyan et al. 2013; Boeche et al. 2013; Anders et al. 2014; Yan et al. 2019). The thin disk generally has a negative radial metallicity gradient (e.g., Bilir et al. 2012; Pilkington et al. 2012; Donor et al. 2020; Katz et al. 2021; Imig et al. 2023), whereas the thick disk has no or positive radial metallicity gradient (e.g., Recio-Blanco et al. 2014; Coskunoğlu et al. 2012; Miranda et al. 2016). For the vertical metallicity gradient, some results suggested that both thin and thick disks have negative values (e.g., Chen et al. 2011; Carrell et al. 2012; Li et al. 2017; Tunçel et al. 2019), while other results tend to suggest a flat gradient for the thick disk (e.g., Katz et al. 2011; Li et al. 2018).

Kinematically and dynamically, the thin disk stars generally have larger orbital rotation velocity, lower velocity dispersion, lower eccentricity and lower maximum distance from the Galactic plane (Z_{max}) than those of the thick disk stars (e.g., Lee et al. 2011; Jing et al. 2016; Mackereth et al. 2019; Robin et al. 2022). The metallicity gradients of orbital rotation velocities are negative and positive for thin and thick disks (e.g., Lee et al. 2011; Han et al. 2020), respectively. The metallicity gradients of eccentricities are positive and negative for thin and thick disks (e.g., Lee et al. 2011; Yan et al. 2019), respectively.

All these distinguished properties for the two disks mean that the thin and thick disks may have experienced different formation mechanisms and evolution histories (e.g., Jenkins 1992; Brook et al. 2004; Schönrich & McMillan 2017; Mackereth et al. 2019; Han et al. 2020).

Spitzer & Schwarzschild (1953) suggested that old stars

¹ Department of Astronomy, Beijing Normal University, Beijing 100875, People's Republic of China; sunweixiang@bnu.edu.cn (WXS); bjjiang@bnu.edu.cn (BWJ).

² South-Western Institute for Astronomy Research, Yunnan University, Kunming 650500, People's Republic of China; x.liu@ynu.edu.cn (XWL).

³ Corresponding authors

will become kinematically hotter with large velocity dispersion as they are scattered by the giant molecular clouds (GMCs). Other studies also revealed that the spiral arms might contribute to their larger velocity dispersion (Barbanis & Woltjer 1967). However, Jenkins (1992) reported that when fully considering the heating of the GMCs and spiral arms, the acceptable heating constant is not enough to explain so kinematically hot properties of the observed old stars. Therefore, the suggestions of violent origins of the thick disk are conceived, including: (i) the thick disk stars formed from heating pre-existing thin disk stars by satellite mergers (e.g., Quinn et al. 1993; Villalobos & Helmi 2008); (ii) the thick disk stars formed by member stars that accreted from satellite galaxies during the merging process (e.g., Abadi et al. 2003); (iii) the thick disk stars formed in an environment with chaotic mergers of gas-rich system (e.g., Brook et al. 2004, 2005, 2007; Bournaud et al. 2009). Recently, studies reported that the inside-out and upside-down star formation (e.g., Kawata et al. 2017; Schönrich & McMillan 2017; Bird et al. 2021), along with a cumulative secular process with stellar migration scenario by churning and blurring (e.g., Loebman et al. 2011; Minchev et al. 2012; Roškar et al. 2012; Kordopatis et al. 2015; Schönrich & McMillan 2017) can also reshape a thick disk component of our Galaxy.

Previous studies (e.g., Lee et al. 2011; Mackereth et al. 2019; Han et al. 2020) suggested that a detailed measurement of chemical, kinematic and dynamic properties of the thin/thick disk is useful for constraining the origin of these stars. However, the observation limitation (e.g., Lee et al. 2011; Bensby, Feltzing & Oey 2014; Mackereth et al. 2019; Han et al. 2020) meant that these properties are not yet well measured in a larger Galactic disk radius which would make a credible assessment of the origins of the thick disk stars. At present, the red clump (RC) stars (e.g., Bovy et al. 2014; Huang et al. 2020) from the APOGEE (Majewski et al. 2017) and LAMOST (e.g., Deng et al. 2012; Cui et al. 2012; Liu et al. 2014; Yuan et al. 2015) surveys present a compelling opportunity for conducting such research. It can be attributed to the significant strengths of these RC stars, including: (i) the luminosities of RC stars are quite stable and are only slightly dependent on age and chemical composition, and therefore can be used as standard candles for the distance indicators (e.g., Cannon 1970; Paczynski & Stanek 1998); (ii) they are widely distributed across the entire Galactic disk, and thus as excellent tracers to study the 3D structures (Bovy et al. 2016), explore the chemical, kinematic and dynamic properties (e.g., Huang et al. 2016; Sun et al. 2020, 2023, 2024), and reveal the assemblage history of the Galactic disk; (iii) the high-precision measurements of the chemical and kinematic parameters (i.e., 3D velocities, 3D positions, metallicity and abundances; Bovy et al. 2014; Huang et al. 2020). Leveraging these samples, it is possible to make an exhaustive analysis of the chemical, kinematic, and dynamic properties of the thin and thick disks over a wider range of Galactocentric radii, thereby enhancing the constraint of the origins of the thin and thick disks. Note that, even though splitting the Galactic disk into "thin" and "thick" components has a long precedence in the literature (e.g., Gilmore & Reid 1983; Fuhrmann 1998; Lee et al. 2011; Mackereth et al. 2019; Han et al. 2020; Sun et al. 2024), it is at least worth mentioning that there are arguments against doing so in favor of a continuous disk model (e.g., Bensby et al. 2007; Bovy et al. 2012a; Kawata & Chappini 2016; Hayden et al. 2017). These samples could also nicely contribute to this debate as well.

This paper is structured as follows. In Section 2, we describe the data used in this study. The metallicity distributions of the thin/thick disks are presented in Section 3, and we investigate the $\Delta V_\phi/\Delta[\text{Fe}/\text{H}]$ and $\Delta\sigma_\phi/\Delta[\text{Fe}/\text{H}]$ distributions of the thin/thick disks in Section 4. In Section 5, we present the distributions of the eccentricities of the thin/thick disks, and the possible formation and evolution history of the thin/thick disks is discussed in Section 6. Finally, our main conclusions are summarized in Section 7.

2. DATA

2.1. The LAMOST and APOGEE RC samples

We mainly use 171,320 primary RC stars (Bovy et al. 2014; Huang et al. 2020) selected from the LAMOST (e.g., Deng et al. 2012; Cui et al. 2012; Liu et al. 2014; Yuan et al. 2015) and APOGEE (Majewski et al. 2017) surveys. These RC stars are selected by using a method based on the large-scale spectroscopic data (e.g., Bovy et al. 2014; Huang et al. 2015, 2020). This method first selected RC-like stars in the metallicity-dependent effective temperature (T_{eff})–surface gravity ($\log g$) plane. Secondly, removing the secondary RC stars from the RC-like stars in the metallicity ($[Z]$)–color ($(J - K_s)_0$) plane. For the APOGEE RC stars (e.g., Bovy et al. 2014), the selection of the RC-like stars used the cuts of $1.8 \leq \log g \leq 0.0018 \text{ dex K}^{-1} (T_{\text{eff}} - T_{\text{eff}}^{\text{ref}}) + 2.5$, where $T_{\text{eff}}^{\text{ref}} = -382.5 \text{ K dex}^{-1} [\text{Fe}/\text{H}] + 4607 \text{ K}$. Then removing the secondary RC stars from the RC-like stars using the conditions of $[Z] > 1.21 [(J - K_s)_0 - 0.05]^9 + 0.0011$ and $[Z] < 2.58 [(J - K_s)_0 - 0.40]^3 + 0.0034$, with additional bounds of $[Z] \leq 0.06$ and $(J - K_s)_0 \geq 0.5$. For a more detailed analysis of the selection of the APOGEE RC stars, please refer to Bovy et al. (2014). For the LAMOST RC stars, Huang et al. (2015, 2020) developed the method in Bovy et al. (2014) to be suitable for the LAMOST data, the cuts of the selecting RC-like stars to $1.8 \leq \log g \leq 0.0006 \text{ dex K}^{-1} (T_{\text{eff}} - T_{\text{eff}}^{\text{ref}}) + 2.5$, where $T_{\text{eff}}^{\text{ref}} = -873.1 \text{ K dex}^{-1} [\text{Fe}/\text{H}] + 4255 \text{ K}$, with additional bounds of $T_{\text{eff}} \leq 5000 \text{ K}$ and $\log g \leq 2.75$. The conditions of removing the secondary RC stars from the RC-like stars update to $[Z] > 1.21 [(J - K_s)_0 - 0.085]^9 + 0.0011$ and $[Z] < 2.58 [(J - K_s)_0 - 0.400]^3 + 0.0034$. For details on the selection of the LAMOST RC stars, please refer to Huang et al. (2015, 2020). By selecting the sources with large signal-to-noise ratio (SNR) for the common targets of the LAMOST and APOGEE RC stars, 177,123 primary RC stars are further selected, 137,448 primary RC stars from LAMOST and 39,675 primary RC stars from APOGEE.

The stellar parameters, such as, T_{eff} , $\log g$, metallicity ($[\text{Fe}/\text{H}]$) and $[\alpha/\text{Fe}]$, of the APOGEE and LAMOST data, are determined by the ASPCAP (e.g., García Pérez et al. 2016) and LSP3 pipelines (e.g., Xiang et al. 2015), respectively. With various tests, the typical uncertainties of the T_{eff} , $\log g$, $[\text{Fe}/\text{H}]$ and $[\alpha/\text{Fe}]$ for the LAMOST sample stars, are respectively better than around, 100 K, 0.10 dex, 0.10–0.15 dex and 0.03–0.05 dex, for the APOGEE sample stars, the uncertainties are slightly smaller (see Bovy et al. 2014; Xiang et al. 2015; García Pérez et al. 2016; Huang et al. 2020). Due to the standard candle nature of the RC stars, the distance errors are around 5%–10%. To ensure the accuracy of the kinematic and dynamic calculations, the astrometric parameters (e.g., proper motions) of the sample stars are updated by using the Gaia DR3 catalog (e.g., Gaia Collaboration et al. 2023a,b; Recio-

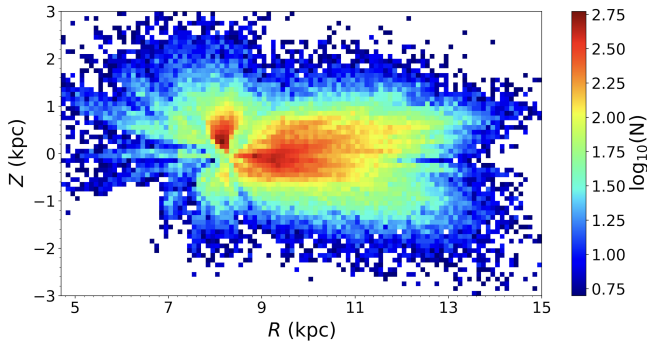


Figure 1. Spatial distribution in the $R - Z$ plane, of the sample stars, with color-coded by the stellar number density. There is a minimum of 8 stars per bin spaced 0.1 kpc in both axes.

Blanco et al. 2023).

2.2. Coordinate Systems and Sample Selections

The standard Galactocentric cylindrical coordinates (R, ϕ, Z) are adopted, and the 3 velocity components are V_R , V_ϕ and V_Z , respectively. To estimate the kinematics and orbits, the Galactocentric distance of the Sun, the local circular velocity and the solar motions are set to be $R_\odot = 8.34$ kpc (Reid et al. 2014), $V_{c,R_\odot} = 238.0$ km s $^{-1}$ (e.g., Reid & Brunthaler 2004; Schönrich et al. 2010, 2012; Reid et al. 2014; Huang et al. 2015, 2016; Bland-Hawthorn & Gerhard 2016), and $(U_\odot, V_\odot, W_\odot) = (13.00, 12.24, 7.24)$ km s $^{-1}$ (Schönrich & Dehnen 2018), respectively. The orbital parameters (i.e. the eccentricity) of each star are determined by *Galpy* (Bovy 2015), under the Galactic gravitational potential as “*MWPotential2014*”. To further ensure the accuracy of the kinematics and dynamics, the following cuts are used for the sample stars:

- LAMOST and APOGEE spectral SNRs ≥ 20 ;
- Distance error $\leq 10\%$;
- $[\text{Fe}/\text{H}] \geq -1.0$ dex and $|V_Z| \leq 120$ km s $^{-1}$.

The first two cuts ensure the uncertainties of the 3D velocities of the sample stars are generally within 5.0 km s $^{-1}$. The last cut is used to exclude the halo stars (e.g., Huang et al. 2018; Hayden et al. 2020; Sun et al. 2020). By the above cuts, 170,729 RC stars are finally selected, of which 39,112 and 131,617 stars are respectively from the APOGEE and LAMOST survey. The spatial distribution of the final selected stars is shown in Fig. 1. Since the $[\text{Fe}/\text{H}]$ and $[\alpha/\text{Fe}]$ are typically different for the two datasets, considering that the LAMOST has a larger sample size than the APOGEE, we further calibrate these parameters of the APOGEE dataset to the LAMOST system based on the best linear fit as displayed in Fig. 2.

2.3. The thin and thick disks of the RC sample

Since the spatial distributions and kinematics of stars can be modified over time, while the atmospheric chemical abundance of stars is generally invariant, we separate the thin and thick disks by using $[\alpha/\text{Fe}]$ ratio. The $[\text{Fe}/\text{H}] - [\alpha/\text{Fe}]$ relation of our sample stars is shown in Fig. 3. The plot shows clearly two branches, which are respectively the thin and thick disks. To get pure thin and thick disks, inspired from previous work (e.g., Bensby et al. 2005; Lee et al. 2011; Brook et al. 2012;

Haywood et al. 2013; Recio-Blanco et al. 2014; Nidever et al. 2014; Guiglion et al. 2015; Hayden et al. 2015; Queiroz et al. 2020; Sun et al. 2023, 2024), two empirical cuts (see Fig. 3) are applied to select the thick disk (23,168 stars above the upper cut) and thin disk (135,009 stars below the lower cut), and the properties of these two disks are presented in details in Table 1.

The histograms of the fractional number density of the distributions for vertical and radial directions, metallicity and V_ϕ are shown in Fig. 4. The results indicate that the thin disk stars are mainly distributed within $|Z| < 3.0$ kpc, while the thick disk stars have a relatively extended distribution with the stellar height extending to up to $|Z| \sim 5.0$ kpc. This is in rough agreement with the nature of the scale-height of the thin disk (typically suggested as $h_z = 0.3 - 0.6$ kpc; e.g., Bovy et al. 2012b; Bland-Hawthorn et al. 2018) is smaller than that of the thick disk (typically suggested as $h_z = 0.8 - 1.0$ kpc; e.g., Bovy et al. 2012b; Bland-Hawthorn et al. 2018). For the radial direction, the thick disk stars peak around 8.0 kpc, while the thin disk stars peak around a much larger Galactic radius, that is, $R \sim 9.5$ kpc, which is in line with the scale-length of the thin disk (typically suggested as 2.5–3.6 kpc; e.g., Bovy et al. 2012b; Hayden et al. 2015) is larger than that of the thick disk (typically suggested as 1.8–2.2 kpc; e.g., Bensby et al. 2011; Bovy et al. 2012b; Hayden et al. 2015). The $[\text{Fe}/\text{H}]$ of the thin and thick disks respectively peaks around -0.2 dex and -0.5 dex, which is consistent with previous studies (e.g., Lee et al. 2011; Haywood et al. 2013; Sun et al. 2020, 2023). The orbital velocity of the thin disk ($V_\phi \sim 230$ km s $^{-1}$) is larger than the thick disk ($V_\phi \sim 195$ km s $^{-1}$), which is also in rough agreement with recent results (e.g., Lee et al. 2011; Sun et al. 2024). This behavior indicates that the asymmetric drift of thick disk stars is generally stronger than thin disk stars. It is worth noting that we do not correct the selection effect for the analyses in Fig. 4, and some features caused by the selection effects are visible, as an example, the double-peaked radial distribution of the thin disk stars (see upper right of Fig. 4).

3. METALLICITY DISTRIBUTION OF THE THIN AND THICK DISKS

The results of the metallicity distributions of thin/thick disks are shown in Figs. 5–7. The thin disk shows obvious radial and vertical trends in $[\text{Fe}/\text{H}]$, which decreases with R (or $|Z|$). The thick disk shows a weak decreasing trend in $[\text{Fe}/\text{H}]$ with $|Z|$, while has no obvious trend with R (see Fig. 5). The $[\text{Fe}/\text{H}] - R$ profile of the thin disk (see Fig. 6) shows significant differences for various Z layers, with the trend becoming flat as R increases. The global profiles break at R around 8.5 kpc, especially for $Z = [1.0, 1.5]$ kpc (orange curve) and $Z = [1.5, 2.0]$ kpc (red curve), the $[\text{Fe}/\text{H}]$ shows an increasing/flat trend with R . Although the number of stars in this region is small, the limitation of the number of stars in each bin (no less than 30 stars) still ensures the statistical reliability. Therefore, the contamination by the thick disk stars may be the possible reason for the $R_{\text{break}} \sim 8.5$ kpc since the flat or inverse/increasing trends at $R \geq 8.5$ kpc (see Fig. 6). Previous studies also suggested the radial metallicity profile breaks at the outer disk (e.g., Spina et al. 2021; Yong et al. 2012; Donor et al. 2020), this break in this work is also traced with $R_{\text{break}} \sim 13.0$ kpc (see Fig. 6) and is in good agreement with Spina et al. (2021). Since the cut-off radius of the disk star formation is generally suggested not to be larger than ~ 14.0 kpc (Schönrich & McMillan 2017), the flared migrators may be the possible reason for this break. The profiles of $[\text{Fe}/\text{H}] - |Z|$

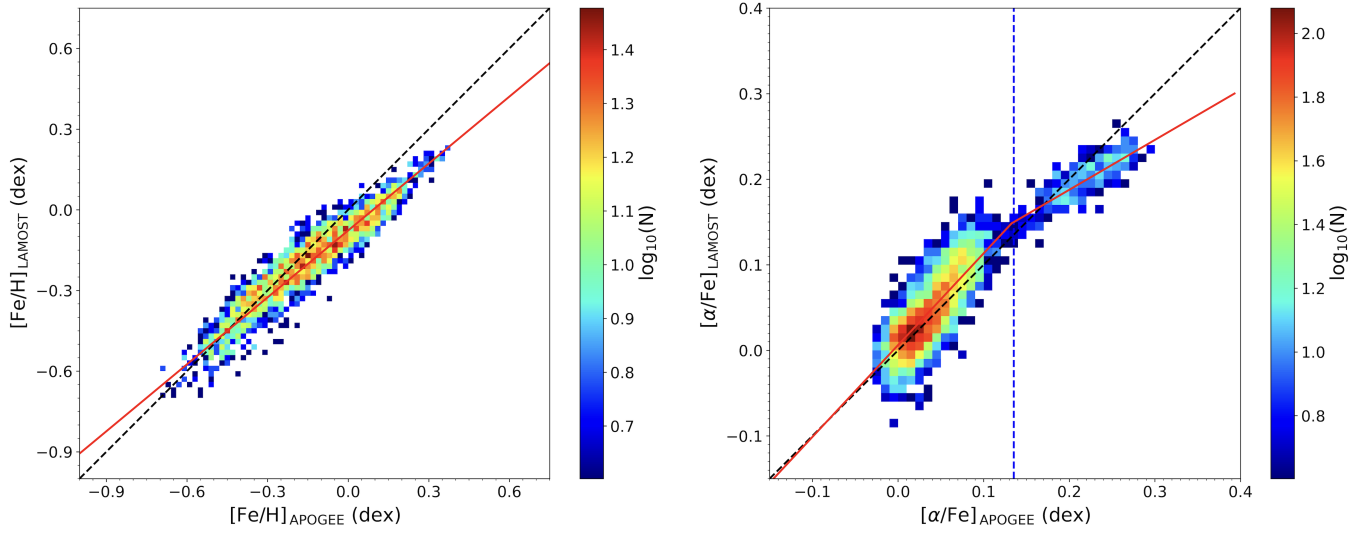


Figure 2. The $[\text{Fe}/\text{H}]$ (left panel) and $[\alpha/\text{Fe}]$ (right panel) calibrations between the APOGEE and LAMOST datasets. Black dashed lines represent the one-to-one relations, and the red solid lines are linear fits to the data. There is a minimum of 4 stars per bin, with the $[\text{Fe}/\text{H}]$ and $[\alpha/\text{Fe}]$ respectively spaced in 0.02 dex and 0.02 dex.

Table 1
The properties of the thin/thick disks

Name	$\langle [\alpha/\text{Fe}] \rangle$ (dex)	$\langle [\text{Fe}/\text{H}] \rangle$ (dex)	$\langle R \rangle$ (kpc)	$\langle V_\phi \rangle$ (km s^{-1})	σ_ϕ (km s^{-1})	Number	Fraction
Thin disk	0.03	-0.2	10.14	225.01	22.97	135,009	79.08%
Thick disk	0.20	-0.4	8.54	179.27	54.81	23,168	13.57%

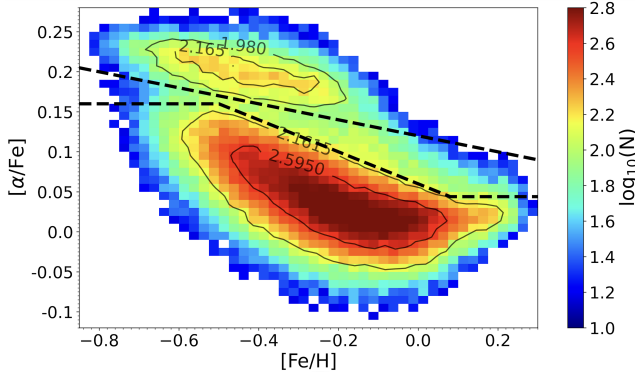


Figure 3. The $[\text{Fe}/\text{H}]$ – $[\alpha/\text{Fe}]$ distribution of the final sample stars, overplotted with contours of equal densities, color-coded by the logarithmic number density. The horizontal axis and vertical axis are respectively spaced by 0.025 dex and 0.02 dex, with a minimum of 15 stars per bin. The two dashed lines are used to separate the thick (above the lines) and the thin (below the lines) disk stars.

of the thin disk show a linear function shape, with the trend becoming flat as R increases (see Fig. 6).

The results of $\Delta[\text{Fe}/\text{H}]/\Delta R$ as function of $|Z|$ and the $\Delta[\text{Fe}/\text{H}]/\Delta|Z|$ as function of R , of the thin/thick disks, are shown in Fig. 7. For $\Delta[\text{Fe}/\text{H}]/\Delta R$, the thin disk shows an increasing trend with $|Z|$, rising from around $-0.06 \text{ dex kpc}^{-1}$ at $|Z| < 0.25 \text{ kpc}$ to $-0.02 \text{ dex kpc}^{-1}$ at $|Z| > 2.75 \text{ kpc}$. The

thick disk is generally weaker than $\sim 0.01 \text{ dex kpc}^{-1}$, and shows no obvious change with $|Z|$, which is in rough agreement with the result of old/high- α populations (e.g., Imig et al. 2023). This may be understood because strong migration can wipe out any possible original gradients. However, the positive $\Delta[\text{Fe}/\text{H}]/\Delta R$ of the thick disk (this positive gradient has been also observed in other works, e.g., Vickers et al. 2021; Imig et al. 2023) is surprising, it means that we do seem to see some evidence of the inside-out star formation and the stars are not fully mixed up to now. In addition, the $\Delta[\text{Fe}/\text{H}]/\Delta R$ of the thin disk is obviously stronger in the south disk than the north disk.

Using a suite of cosmological chemo-dynamical disk galaxy simulations, Miranda et al. (2016) reported $\Delta[\text{Fe}/\text{H}]/\Delta R$ as a function of $|Z|$ for thin and thick disks of the Milky Way-like galaxies simulated in a cosmological context, at $5.0 < R < 10.0 \text{ kpc}$. For thin disk, Miranda et al. (2016) suggested the thin disk in the region of $|Z| = 1.0$ – 1.5 kpc has $\Delta[\text{Fe}/\text{H}]/\Delta R = -0.028 \text{ dex kpc}^{-1}$. This result is in good agreement with ours for the thin disk in the north with $|Z| = 1.0$ – 1.5 kpc (see upper left panel of Fig. 7). Their thin disk result outside the region of $|Z| = 1.0$ – 1.5 kpc is obviously different from ours, which may be caused by the condition with $5.0 < R < 10.0 \text{ kpc}$ of Miranda et al. (2016). It is worth mentioning that our thin disk results in the region of $|Z| = 0.0$ – 0.5 are in rough agreement with Pilkington et al. (2012), who reported the young population of the galaxies selected from the RaDES (Ramses Disk Environment Study)

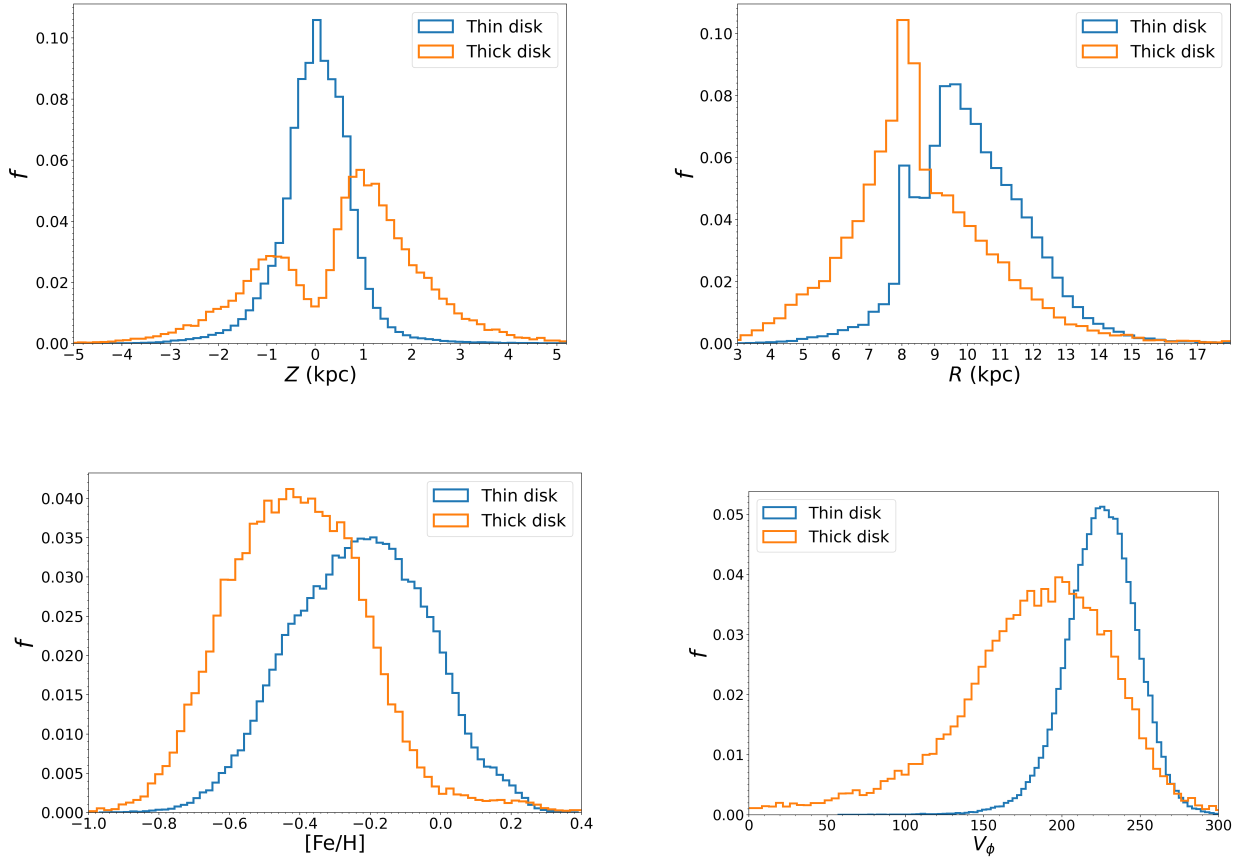


Figure 4. Fractional number density ($f = N_i/N_{\text{tot}}$) distributions of the vertical direction (upper left), radial direction (upper right), $[Fe/H]$ (bottom left) and V_ϕ (bottom right), for the thin and thick disks. In which, N_i is the number of stars in the i -th radial/vertical bin and N_{tot} is the total number of stars of the individual population. Different color lines represent different populations that are marked as labels in the top corner.

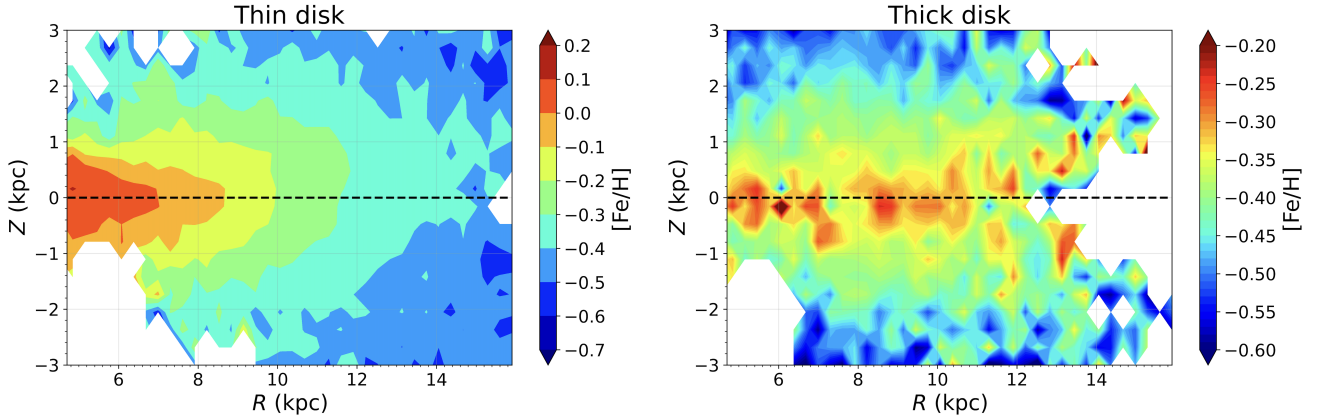


Figure 5. Metallicity distribution, in the R - Z plane, of the thin (left panel) and thick (right panel) disks.

has $\Delta[Fe/H]/\Delta R = -0.059 \text{ dex kpc}^{-1}$. For thick disk, the results with $|Z| < 1.5 \text{ kpc}$ of Miranda et al. (2016), are in good agreement with ours, while their gradients at $|Z| > 1.5 \text{ kpc}$ are obviously stronger than our results (see upper right panel of Fig. 7), while it is in good agreement with the metallicity gradient in guiding radius (R_g) of the thick disk in Vickers et al. (2021). These differences may be related to the stellar migration of the thick disk stars (e.g., Sellwood & Binney 2002;

Han et al. 2020; Vickers et al. 2021).

For $\Delta[Fe/H]/\Delta|Z|$, the thin disk shows an increasing trend with R in the form of a single power law, which increases steadily from around $-0.36 \text{ dex kpc}^{-1}$ at $R \sim 5.5 \text{ kpc}$ to around $-0.05 \text{ dex kpc}^{-1}$ at $R > 11.5 \text{ kpc}$. The thick disk displays a similar gradient (nearly $-0.06 \sim -0.08 \text{ dex kpc}^{-1}$) for all R bins.

We fit the profiles of the $\Delta[Fe/H]/\Delta|Z|$ - R for the thin/thick

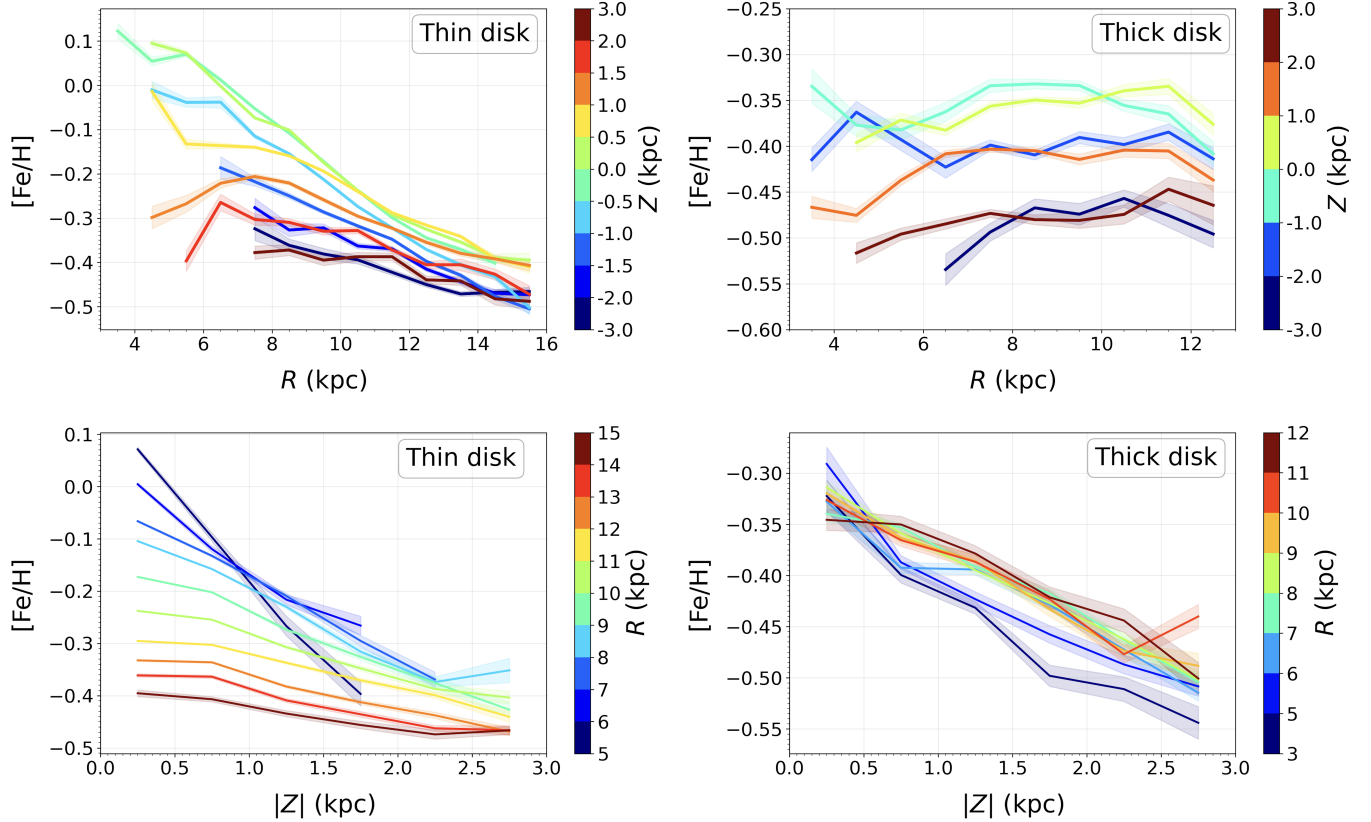


Figure 6. Radial (upper panels) and vertical (bottom panels) metallicity profiles of the thin (left panels) and thick (right panels) disks.

disks (see Fig. 7), which yields $\Delta[\text{Fe}/\text{H}]/\Delta|Z| \propto R^{-2.307}$ and $\Delta[\text{Fe}/\text{H}]/\Delta|Z| = 0.001 R - 0.078$ for the thin and thick disks, respectively (to distinguish it from the original data, hereafter, we name the profiles of $\Delta[\text{Fe}/\text{H}]/\Delta|Z|$ as $\text{Fit}_\Delta[\text{Fe}/\text{H}]/\Delta|Z|$). After subtracting the fitted profile of the original data, we present the correction vertical metallicity gradient ($\text{Cor}_\Delta[\text{Fe}/\text{H}]/\Delta|Z| = \Delta[\text{Fe}/\text{H}]/\Delta|Z| - \text{Fit}_\Delta[\text{Fe}/\text{H}]/\Delta|Z|$) as a function of R in Fig. 8. The result indicates the $\text{Cor}_\Delta[\text{Fe}/\text{H}]/\Delta|Z|$ exhibits some oscillation with R for the thin and thick disks. The resonances with the Galactic bar are the most possible reason for these oscillations (e.g., Kalnajs 1991; Dehnen 2000; Antoja et al. 2014; Hunt et al. 2018; Sun et al. 2023).

A north-south asymmetry in $[\text{Fe}/\text{H}]$ is obvious for the thin disk at $R > 9.0$ kpc (see Fig. 5), which is in rough agreement with the warp in structure (e.g., Momany et al. 2006; Poggio et al. 2018; Mackereth et al. 2019; Li et al. 2020). In further work, we will attempt to establish a correlation between the north-south asymmetry in $[\text{Fe}/\text{H}]$ and the disk warp, and the related study is underway and shall be presented in a separate paper (Sun et al. 2024, in preparation). The north-south asymmetry in $[\text{Fe}/\text{H}]$ signal is weak for the thick disk (see Fig. 5 and upper right panel of Fig. 7), and such asymmetry signal is further weakened but did not disappear when we limit the $[\alpha/\text{Fe}]$ of thick disk stars larger than 0.15 dex. This implies that the thick disk may also have a weak warp signal if the north-south chemical asymmetry is caused by the Galactic warp (e.g., Li et al. 2020; Sun et al. 2024). The weak signal for the thick disk is in good agreement with the old/high- α populations in recent studies (see e.g., Poggio et al. 2018; Sun et al. 2024). This indicates that the metallicity asymmetry (and

the warp) may be a long-lived feature.

4. THE $\Delta V_\phi/\Delta[\text{Fe}/\text{H}]$ AND $\Delta\sigma_\phi/\Delta[\text{Fe}/\text{H}]$ DISTRIBUTIONS OF THE THIN/THICK DISKS

The metallicity gradients of azimuthal velocity and its dispersion provide a more intuitive illustration of the stellar radial migrations (e.g., Lee et al. 2011; Han et al. 2020). Here, we determined the $\Delta V_\phi/\Delta[\text{Fe}/\text{H}]$ and $\Delta\sigma_\phi/\Delta[\text{Fe}/\text{H}]$ as a function of R and Z for the thin and thick disks (see Fig. 9).

For the thin disk, $\Delta V_\phi/\Delta[\text{Fe}/\text{H}]$ shows a global negative value for all R bins. In the solar radius ($8.0 < R \leq 9.0$ kpc), $\Delta V_\phi/\Delta[\text{Fe}/\text{H}]$ is around $-27.48 \pm 1.00 \text{ km s}^{-1} \text{ dex}^{-1}$ at $-1.0 \leq Z < 0.0$ kpc, and is around $-26.81 \pm 0.91 \text{ km s}^{-1} \text{ dex}^{-1}$ at $0.0 \leq Z < 1.0$ kpc. Our result $\Delta V_\phi/\Delta[\text{Fe}/\text{H}] = -27.48 \pm 1.00 \text{ km s}^{-1} \text{ dex}^{-1}$ is in good agreement with the result of Han et al. (2020), who reported that $\Delta V_\phi/\Delta[\text{Fe}/\text{H}]$ is $-28.2 \text{ km s}^{-1} \text{ dex}^{-1}$ for the G- and K-dwarfs in the solar neighborhood. The $\Delta\sigma_\phi/\Delta[\text{Fe}/\text{H}]$ shows a slight increasing trend with R , rising from $\Delta\sigma_\phi/\Delta[\text{Fe}/\text{H}] \sim -10.0 \text{ km s}^{-1} \text{ dex}^{-1} \text{ kpc}^{-1}$ at $R \sim 7.0$ kpc to $\Delta\sigma_\phi/\Delta[\text{Fe}/\text{H}] \sim 20.0 \text{ km s}^{-1} \text{ dex}^{-1} \text{ kpc}^{-1}$ at R larger than ~ 15.0 kpc. For the thick disk, $\Delta V_\phi/\Delta[\text{Fe}/\text{H}]$ and $\Delta\sigma_\phi/\Delta[\text{Fe}/\text{H}]$ are respectively positive and negative. The $\Delta\sigma_\phi/\Delta[\text{Fe}/\text{H}]$ for the thick disk is globally stronger than that for the thin disk.

The $\Delta V_\phi/\Delta[\text{Fe}/\text{H}]$ is respectively negative and positive for thin and thick disks is interesting. To explain this behavior, it is necessary to clarify the meaning of churning and blurring in the ‘radial migration’ terms in the following analysis. In churning, the angular momentum of stellar orbit changes due to the interaction of the Galactic non-asymmetric structure (i.e., the Galactic bar or spiral arms), and the change of

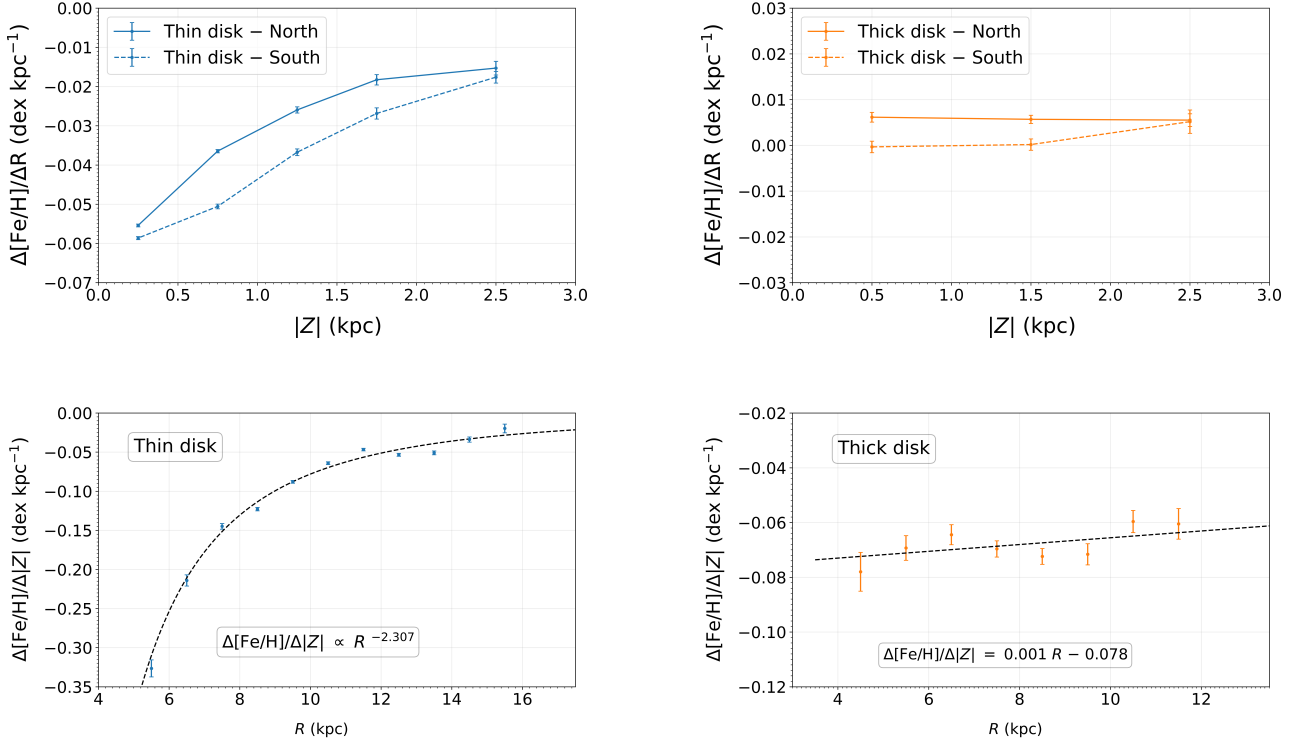


Figure 7. The $\Delta[\text{Fe}/\text{H}]/\Delta R$ as a function of the $|Z|$ of the thin (upper left) and thick (upper right) disks, and the $\Delta[\text{Fe}/\text{H}]/\Delta|Z|$ as a function of the R of thin (bottom left) and thick (bottom right) disks.

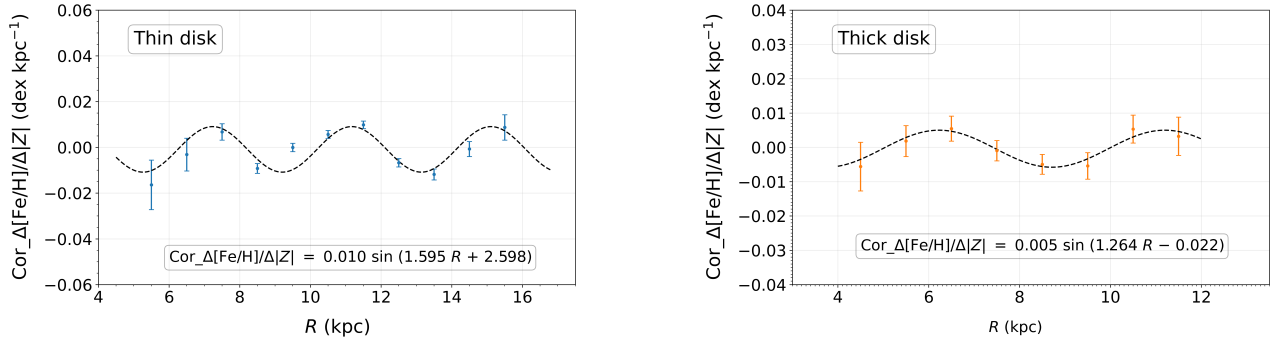


Figure 8. The correction vertical metallicity gradient as a function of R for the thin (left panel) and thick (right panel) disks.

the stellar angular momentum leads to the change of the stellar guiding radius, and so as leads to stellar radial migration (e.g., Sellwood & Binney 2002; Schönrich & McMillan 2017; Hayden et al. 2020). In blurring, stellar kinematics become heated (by scattering of the GMCs, and resonance between the Galactic bar and spiral arms) with time, resulting in stellar radial velocity dispersion rising with time, and the larger radial velocity dispersion of stars leads to large epicyclic motions over their orbits with the angular momentum of each star conserved (e.g., Minchev & Famaey 2010; Schönrich & McMillan 2017; Hayden et al. 2020).

The negative $\Delta V_\phi/\Delta[\text{Fe}/\text{H}]$ of the thin disk is widely reported by previous studies in the solar neighborhood (e.g., Spagna et al. 2010; Lee et al. 2011; Recio-Blanco et al. 2014; Kordopatis et al. 2017; Hayden et al. 2020; Han et al. 2020).

Due to the negative radial metallicity gradient of the thin disk stars (see Fig. 5-7), stars with richer metallicity generally have smaller Galactic guiding radii and move outward with a blurring radial mixing mechanism that leads these stars to be observed with lower azimuthal velocities than local stars, while stars formed in the outer Galactic disk generally have lower metallicity and higher azimuthal velocities than those of local stars, thus resulting in negative $\Delta V_\phi/\Delta[\text{Fe}/\text{H}]$.

For the thick disk stars, the inside-out and upside-down formation of the thick disk (e.g., Kawata et al. 2017; Schönrich & McMillan 2017), along with the stellar radial migration (e.g., Zhang et al. 2020; Han et al. 2020), can easily explain the observed results. As the radial velocity dispersion is quite large for thick disk stars (e.g., Lee et al. 2011; Hayden et al. 2020; Sun et al. 2024), these stars experience obvious ra-

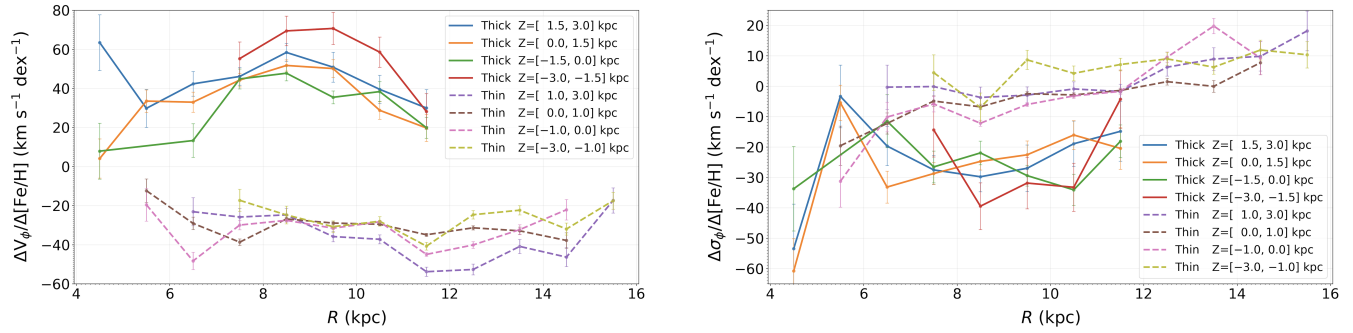


Figure 9. Metallicity gradients of the azimuthal velocity (left panel) and azimuthal velocity dispersion (right panel) as a function of R and Z .

dial epicyclic motion which results in lower V_ϕ as they move outwards. As the radial velocity dispersion is smaller for the more metal-rich thick disk stars than that for the metal-poor stars (e.g., Hayden et al. 2020; Sun et al. 2024), this causes smaller radial epicyclic motion and larger V_ϕ for the metal-rich stars than those for the metal-poor stars. Combined with stellar positive radial metallicity gradient (see Fig. 6–7), we can well explain the relations of the metallicity with V_ϕ and σ_ϕ .

The $V_\phi/\Delta[\text{Fe}/\text{H}]$ of the thin disk shows a global slight increasing trend with R at $R > 11.5$ kpc (see left panel of Fig. 9). We consider some possible explanations that can explain this behavior: (i) Stars in this region are generally dominated by migrators that formed in the inner disk, metal-rich stars generally have experienced larger radial epicyclic motion than those of metal-poor stars, and so as lead to a strong gradient; (ii) churning as the likely mechanism of radial mixing for a significant number of stars in this region; (iii) the flared nature (e.g., Minchev et al. 2015; Bovy et al. 2016; Sun et al. 2020; Vickers et al. 2021) in the outer Galactic disk. The increasing trend of $\Delta\sigma_\phi/\Delta[\text{Fe}/\text{H}]-R$ for the thin disk (see right panel of Fig. 9), may be linked to the warped disk.

5. ECCENTRICITY DISTRIBUTIONS OF THE THIN/THICK DISKS

Different dynamic heating processes can be clearly detected in the properties of chemo-dynamics (e.g., Quinn et al. 1993; Abadi et al. 2003; Brook et al. 2004; Sales et al. 2009; Schönrich & Binney 2009; Loebman et al. 2011; Minchev et al. 2012; Schönrich & McMillan 2017). Here, we present the distributions of the eccentricities of different $[\alpha/\text{Fe}]$ populations in Fig. 10. For the thin disk, all the various $[\alpha/\text{Fe}]$ sub-populations peak around 0.1 in eccentricities, with similar distribution shapes. It is somewhat surprising that the thin disk with $0.15 \leq [\alpha/\text{Fe}] < 0.25$ in panel (d) seems to have some stars with high eccentricities (typically larger than ~ 0.4). The “young” $[\alpha/\text{Fe}]$ -enhanced stars (e.g., Chiappini et al. 2015; Martig et al. 2015; Jofré et al. 2016; Yong et al. 2016; Matsuno et al. 2018; Hekker & Johnson 2019; Sun et al. 2020) can explain some of these stars, and the contamination of the thick disk stars also would contribute a substantial amount.

For the thick disk, the eccentricity distributions are distinguished for different $[\alpha/\text{Fe}]$ sub-populations in that the $0.05 \leq [\alpha/\text{Fe}] < 0.15$, $0.15 \leq [\alpha/\text{Fe}] < 0.25$ and $[\alpha/\text{Fe}] \geq 0.25$ populations are respectively peaked around, 0.18, 0.25 and 0.3. In panel (e), the distributions seem to show weak double peaks, with the second peak at around 0.9. In comparison with the simulations of Sales et al. (2009) who predicted the distributions of the eccentricities by heating, accretion, migration and

merger, our results indicate that the thick disk stars in panels (c), (d) and (e), are respectively, mainly heated by migration, gas-rich mergers and accretion. In addition, the heating by migration is indispensable for both thin and thick disks.

6. DISCUSSION ON THE FORMATION AND EVOLUTION OF THE GALACTIC DISK

These distinguished properties of the thin and thick disks have been widely measured and characterized by previous studies (e.g., Fuhrmann 1998; Bensby et al. 2005; Lee et al. 2011; Yan et al. 2019; Han et al. 2020; Sun et al. 2024). These results indicate the thin and thick disks may have experienced different formation mechanisms and/or evolution histories (e.g., Jenkins 1992; Brook et al. 2004; Mackereth et al. 2019; Han et al. 2020). Briefly summarizing, the thin disk is widely considered to originate from dynamic heating by both GMCs and spiral arms (e.g., Spitzer & Schwarzschild 1953; Jenkins 1992; Mackereth et al. 2019), and the disk warp, flare, bending, and some perturbation events also contributed an amount for the heating of the thin disk stars (e.g., Khoperskov & Bertin 2017; Mackereth et al. 2019; Sun et al. 2024). For thick disk, the “inside-out” and “upside-down” stars formation, along with radial migration, can readily understand the observed properties (e.g., Schönrich & McMillan 2017; Vickers et al. 2021; Han et al. 2020). Several studies also revealed that the thick disk stars also require a significant contribution from some violent heating mechanisms, such as merger (e.g., Quinn et al. 1993; Villalobos & Helmi 2008) and accretion (e.g., Abadi et al. 2003), or born in the chaotic mergers of gas-rich systems and/or turbulent interstellar medium (e.g., Brook et al. 2004; Wisnioski et al. 2015). The “two-infall” (e.g., Chiappini et al. 1997; Spitoni et al. 2019; Lian et al. 2020) and a clumpy stars formation (e.g., Bournaud et al. 2007; Clarke et al. 2019; Amarante et al. 2020) models can also explain the thick disk stars.

Since the existing simulations/models are affected by many factors, i.e., some assumptions and unavoidable numerical bias, the simulations/models for the formation and evolution of the disk may be an incomplete physical reality, and hence, the comparison of our results with simulations/models cannot be well quantized. Therefore, we only compare qualitatively our results with expectations from the results of the simulations/models that are related to radial migration, merger, accretion, gas-rich systems and other disk heating simulations/models.

For the thin disk, the radial migration simulations/models (e.g., Sellwood & Binney 2002; Schönrich & Binney 2009; Minchev & Famaey 2010; Schönrich & McMillan 2017) predict that gas density in the inner disk is higher (therefore the

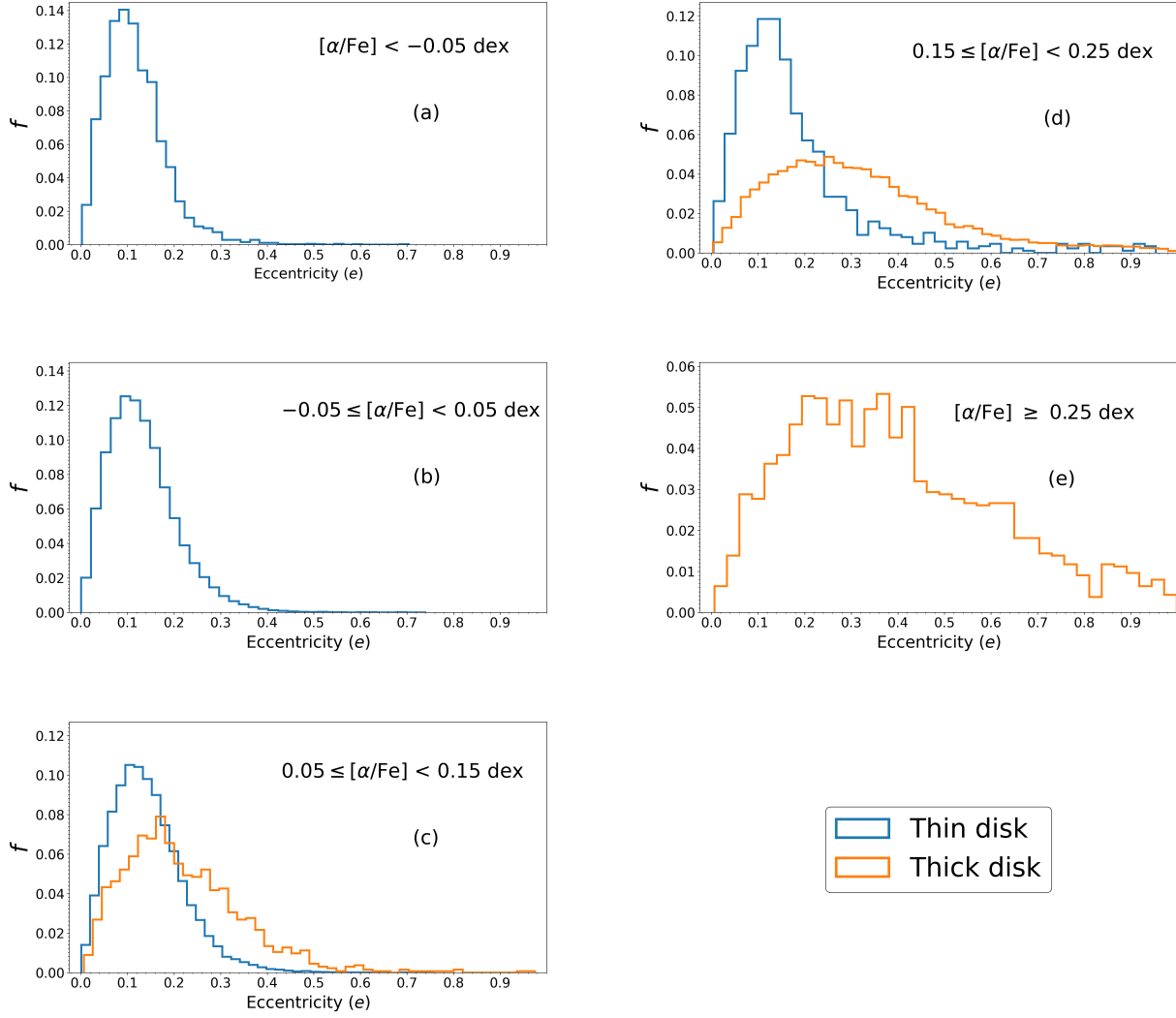


Figure 10. Histograms of eccentricities for the thin-disk (black line) and thick-disk (red line) stars in different $[\alpha/\text{Fe}]$ bins, as indicated in the legends of each panel. The $[\alpha/\text{Fe}]$ range increases from panels (a) to (e).

$[\text{Fe}/\text{H}]$ is richer) than the outer disk for the thin disk. Thus, stars born in the inner disk are richer in $[\text{Fe}/\text{H}]$ than in the outer disk. This means the thin disk has an initial negative metallicity gradient with R in the earlier times. These stars could be changed by radial migration, which results in a flat radial metallicity gradient. Loebman et al. (2011) reported a weak radial metallicity with $\Delta[\text{Fe}/\text{H}]/\Delta R = -0.02 \text{ dex kpc}^{-1}$ for the thin disk in the solar neighborhood ($R = 7\text{--}11 \text{ kpc}$ and $Z = 0.3\text{--}2.0 \text{ kpc}$), by using N-body simulations of radial migration. This result is in good agreement with ours for the thin disk in the north with $Z = 1.5 \sim 2.0 \text{ kpc}$ and in the south with $Z = -2.5 \sim -2.0 \text{ kpc}$ (see Fig. 7). Furthermore, Loebman et al. (2011) also reported the thin disk in the region of $R = 7\text{--}9 \text{ kpc}$ and $|Z| = 0.1\text{--}1 \text{ kpc}$ has $\Delta V_\phi/\Delta[\text{Fe}/\text{H}] = -19.03 \text{ km s}^{-1} \text{ dex}^{-1}$. This result is weaker than our gradient with $\Delta V/\Delta[\text{Fe}/\text{H}] = -26.81 \pm 0.91 \text{ km s}^{-1} \text{ dex}^{-1}$ (see Fig. 9), while our result is well consistent with the result from Han et al. (2020) with $\Delta V/\Delta[\text{Fe}/\text{H}] = -27.48 \pm 1.00 \text{ km s}^{-1} \text{ dex}^{-1}$. Thus, we consider that the $\Delta[\text{Fe}/\text{H}]/\Delta R$ of the thin disk can be well explained by the global radial migration simulations/models, while our result of $\Delta V/\Delta[\text{Fe}/\text{H}]$

of the thin disk indicates that the radial migration may be only one of the multiple contributions. The difference of the relation of $\Delta[\text{Fe}/\text{H}]/\Delta R$ vs. $|Z|$ (see upper left panel of Fig. 7) shows that the $\Delta[\text{Fe}/\text{H}]/\Delta R$ of the thin disk is obvious stronger for the south disk than that for the north disk, indicating that the disk may have experienced some turbulent events from south to north (e.g., Gómez et al. 2012a,b; Laporte et al. 2018; Carrillo et al. 2019; Sun et al. 2024), and/or may be linked to the disk warp (e.g., Momany et al. 2006; Gaia Collaboration et al. 2018). The oscillations of the $\text{Cor.} \Delta[\text{Fe}/\text{H}]/\Delta|Z|$ with R for the thin and thick disks may indicate the resonance with the Galactic Bar. The trend of the $\Delta[\text{Fe}/\text{H}]/\Delta R$ with $|Z|$ (and/or the trend of $\Delta[\text{Fe}/\text{H}]/\Delta|Z|$ with R) may be linked to a flared disk (e.g., Minchev et al. 2015; Bovy et al. 2016; Sun et al. 2024).

For the thick disk, Loebman et al. (2011) suggested $\Delta[\text{Fe}/\text{H}]/\Delta R = 0.00 \text{ dex kpc}^{-1}$ and $\Delta[\text{Fe}/\text{H}]/\Delta|Z| = -0.03 \text{ dex kpc}^{-1}$ by the N-body simulation of radial migration. Their radial metallicity gradient is well consistent with our results (see upper right panel of Fig. 7), while their vertical metallicity gradient is slightly smaller than our

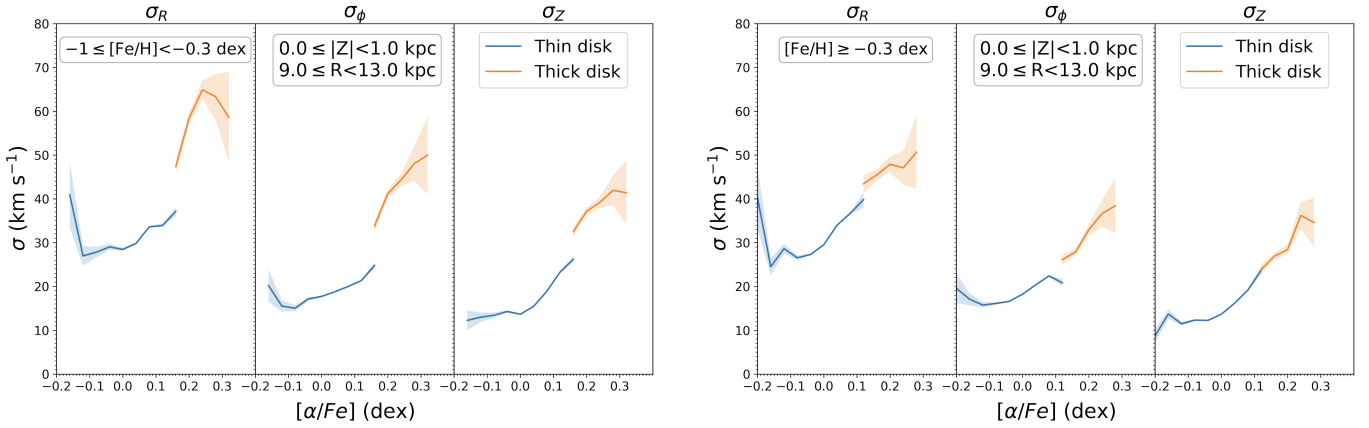


Figure 11. The $[\alpha/\text{Fe}]$ –velocity dispersion for the metal-poor (left panel) and metal-rich (right panel) populations.

result of $\Delta[\text{Fe}/\text{H}]/\Delta|Z| = -0.06 \sim -0.08 \text{ dex kpc}^{-1}$ (see bottom panel of Fig. 7). The suggested $\Delta V/\Delta[\text{Fe}/\text{H}]$ as $+8.0 \text{ km s}^{-1} \text{ dex}^{-1}$ by the simulations/models of radial migration (Loebman et al. 2011) is also obviously smaller than our result (see Fig. 9). From the simulations/models of Sales et al. (2009), the fraction of high eccentricity ($e > 0.5$) thick disk stars formed by radial migration heating mechanism is apparently less than our results as exhibited in Fig. 10. These results indicate that the radial migration contributes just some amount to the formation and evolution of the thick disk, but does not dominate. Thus, some additional star formation and heating mechanisms of the thick disk may be more in line with our measurements. The global positive $\Delta V_\phi/\Delta[\text{Fe}/\text{H}]$ and $\Delta[\text{Fe}/\text{H}]/\Delta R$ of the thick disk (Fig. 8–9) may be some indication of the “inside-out” and “upside-down” star formation scenario (e.g., Kawata et al. 2017; Schönrich & McMillan 2017). The eccentricity distributions indicate that thick disk stars have experienced some violent heating processes, such as migration, merger and accretion (see Fig. 10). The trend of the $\Delta V_\phi/\Delta[\text{Fe}/\text{H}]$ (and/or $\Delta\sigma_\phi/\Delta[\text{Fe}/\text{H}]$) with R may indicate a warped thick disk (e.g., Li et al. 2020; Sun et al. 2024).

The $[\alpha/\text{Fe}]$ – $[\text{Fe}/\text{H}]$ distribution in our result indicates that the thin and thick disks are non-continuous. This is in good agreement with previous studies (e.g., Fuhrmann 1998; Lee et al. 2011; Han et al. 2020; Sun et al. 2020), and to some extent opposes the continuous disk model (e.g., Bensby et al. 2007; Bovy et al. 2012a; Kawata & Chiappini 2016; Hayden et al. 2017). Our results with non-continuous $[\alpha/\text{Fe}]$ – $[\text{Fe}/\text{H}]$ distribution of the thin and thick disk is well consistent with the predictions of the “two-infall” (e.g., Chiappini et al. 1997; Spitoni et al. 2019; Lian et al. 2020) and the clumpy stars formation (e.g., Bournaud et al. 2007; Clarke et al. 2019; Amante et al. 2020) models. Our measurement radial and vertical profiles of the thick disk (see left panels of Fig 6) are also in line with the results of the clumpy stars formation model in Clarke et al. (2019).

The stellar $[\alpha/\text{Fe}]$ –velocity dispersion (σ) relations are well characterized in the solar neighborhood (e.g., Minchev, Chiappini & Martig 2013; Minchev et al. 2014; Hayden et al. 2020), which provide rich information for the perturbation and heating histories of the Galactic disk (e.g., Minchev et al. 2014; Hayden et al. 2020; Sun et al. 2024). The global increasing trends of the $[\alpha/\text{Fe}]$ – σ are clearly detected for various populations (see Fig. 11), which are likely because of the heating from Giant Molecular Clouds (GMCs) (e.g., Spitzer & Schwarzschild 1951, 1953; Barbanis & Woltjer 1967; Jenk-

ins 1992). The global trend of $\sigma_R > \sigma_\phi > \sigma_z$ at the same $[\alpha/\text{Fe}]$ (see Fig. 11), may point to the heating from transient spiral arms (e.g., Jenkins 1992; Sun et al. 2024).

The trend of the $[\alpha/\text{Fe}]$ – σ relation for the thick disk deviates significantly from the growth trend of the $[\alpha/\text{Fe}]$ – σ relation for the thin disk, showing an obvious gap for the thin and thick disks (see Fig. 11). This result indicates that the thick disk stars may have experienced some violent heating processes, such as the minor mergers, accretions and infall of misaligned gas (e.g., Quinn et al. 1993; Abadi et al. 2003; Roškar et al. 2010; Grand et al. 2016; Kazantzidis et al. 2008; Aumer & White 2013; Belokurov et al. 2018; Deason et al. 2018; Helmi et al. 2018; Kruijssen et al. 2019; Sun et al. 2024). The thick disk shows a flat/weak trend in σ as $[\alpha/\text{Fe}]$ increases at $[\alpha/\text{Fe}] > 0.2 \text{ dex}$, and different $[\alpha/\text{Fe}]$ shows a similar velocity dispersion, which implies that these thick disk stars are possibly formed in the chaotic merger of gas-rich systems and turbulent interstellar medium (ISM) (e.g., Brook et al. 2004, 2007, 2012; Wisnioski et al. 2015; Mackereth et al. 2019; Sun et al. 2024).

As a reminder of the influence of the data uncertainties on our results, although we have tested the reliability of the results in this paper, the impact on the understanding of the assembly history of the Milky Way still can not be completely ruled out. A later complete physical reality simulations/models and higher-precision observations may help us to make a complete understanding of the formation and evolution of the Galactic disk.

7. CONCLUSIONS

Using over 170,000 red clump stars selected from the LAMOST and APOGEE spectroscopic surveys, we make a detailed measurement of the metallicity distributions, kinematics and dynamics of the thin and thick disks mainly between $5.0 \leq R \leq 15.0 \text{ kpc}$ and $|Z| \leq 3.0 \text{ kpc}$ with high accuracy. We find that:

- Thin and thick disks display significant differences in the metallicity, $\Delta V_\phi/\Delta[\text{Fe}/\text{H}]$, $\Delta\sigma_\phi/\Delta[\text{Fe}/\text{H}]$ and eccentricity distributions, as well as the $[\alpha/\text{Fe}]$ –velocity dispersion relations. The spatial variations in $\Delta[\text{Fe}/\text{H}]/\Delta R$ and $\Delta[\text{Fe}/\text{H}]/\Delta|Z|$ of the thin disk are globally stronger than those of the thick disk. The $\Delta V_\phi/\Delta[\text{Fe}/\text{H}]$ is respectively negative and positive for the thin and thick disks, and the $\Delta\sigma_\phi/\Delta[\text{Fe}/\text{H}]$ of the thin disk is globally weaker than the thick disk. The north-south asymmetry in $[\text{Fe}/\text{H}]$ is signif-

icant for the thin disk, whereas the thick disk shows much weaker asymmetry. The $[\alpha/\text{Fe}]$ -velocity dispersion relation of the thin disk shows an increasing trend with $[\alpha/\text{Fe}]$ at its high $[\alpha/\text{Fe}]$ (> 0.05 dex), whereas the thick disk shows a flat trend at its high $[\alpha/\text{Fe}]$ (> 0.2 dex).

- The metallicity distributions indicate that the thin disk is generally steeper in $\Delta[\text{Fe}/\text{H}]/\Delta R$ than the thick disk that the $\Delta[\text{Fe}/\text{H}]/\Delta R$ shows an increasing trend with $|Z|$, rising from $\Delta[\text{Fe}/\text{H}]/\Delta R \sim -0.06$ dex kpc^{-1} at $|Z| < 0.25$ kpc to $\Delta[\text{Fe}/\text{H}]/\Delta R \sim -0.02$ dex kpc^{-1} at $|Z| > 2.75$ kpc. The thick disk shows a global weak positive $\Delta[\text{Fe}/\text{H}]/\Delta R$, generally weaker than 0.01 dex kpc^{-1} , and this gradient shows no obvious change with $|Z|$. The $\Delta[\text{Fe}/\text{H}]/\Delta|Z|$ of the thin disk follows a single power law that increases steadily from around -0.36 dex kpc^{-1} at $R \sim 5.5$ kpc to around -0.05 dex kpc^{-1} at $R > 11.5$ kpc. The thick disk exhibits an almost constant gradient (nearly $-0.06 \sim -0.08$ dex kpc^{-1}) for all R bins. The north-south asymmetry in $[\text{Fe}/\text{H}]$ may be linked to the disk warp and/or the disk perturbation events, and the trend of the $\Delta[\text{Fe}/\text{H}]/\Delta R$ with $|Z|$ (and/or the trend of $\Delta[\text{Fe}/\text{H}]/\Delta|Z|$ with R) may indicate that the disk warp (e.g., Momany et al. 2006; Poggio et al. 2018) and flare (e.g., Minchev et al. 2015; Bovy et al. 2016), as well as the oscillations of the $\text{Cor}_\Delta[\text{Fe}/\text{H}]/\Delta|Z|$ with R for the two disks may be linked to the resonance with the Galactic Bar (e.g., Kalnajs 1991; Dehnen 2000).

- The $\Delta V_\phi/\Delta[\text{Fe}/\text{H}]$ is respectively negative and positive for the thin and thick disks, which may indicate an “inside-out” and “upside-down” (e.g., Kawata et al. 2017; Schönrich & McMillan 2017) star formation mechanism of the thick disk. The $\Delta V_\phi/\Delta[\text{Fe}/\text{H}]$ in our measurement is generally stronger than the predicted results of the radial migration simulations/models (e.g., Sellwood & Binney 2002; Schönrich & McMillan 2017), which indicates that the disk stars may have experienced some turbulent events or have experienced some violent heating processes.

- The eccentricity results indicate that the thick stars with $0.05 \leq [\alpha/\text{Fe}] < 0.15$ dex, $0.15 \leq [\alpha/\text{Fe}] < 0.25$ dex and $[\alpha/\text{Fe}] \geq 0.25$ dex, may have experienced the heating by migration (e.g., Sellwood & Binney 2002; Schönrich & McMillan 2017), merger (e.g., Quinn et al. 1993; Villalobos & Helmi 2008) and accretion (e.g., Abadi et al. 2003), respectively. In addition, both thin and thick disks require a long-term heating by migration.

- The $[\alpha/\text{Fe}]$ -velocity dispersion relations show a global increasing trend, which indicates the dynamical heating of disk stars by scattering of GMCs and spiral arms (e.g., Spitzer & Schwarzschild 1951; Barbanis & Woltjer 1967; Jenkins 1992). A gap detected in the relations of $[\alpha/\text{Fe}]$ -velocity dispersion of thin and thick disks is likely because the thick disk stars may be heated by merger and accretion, or the thick disk stars were born in the chaotic mergers of gas-rich systems and/or turbulent ISM (e.g., Brook et al. 2004; Wisnioski et al. 2015).

ACKNOWLEDGEMENTS

We thank the anonymous referee for very useful suggestions to improve the work. This work is supported by the NSFC projects 12133002, and National Key R&D Program

of China No. 2019YFA0405503, and CMS-CSST-2021-A09, and National Natural Science Foundation of China grants 12073070, and 12003027.

Guoshoujing Telescope (the Large Sky Area Multi-Object Fiber Spectroscopic Telescope LAMOST) is a National Major Scientific Project built by the Chinese Academy of Sciences. Funding for the project has been provided by the National Development and Reform Commission. LAMOST is operated and managed by the National Astronomical Observatories, Chinese Academy of Sciences. The LAMOST FELLOWSHIP is supported by Special Funding for Advanced Users, budgeted and administrated by Center for Astronomical Mega-Science, Chinese Academy of Sciences (CAMS)

REFERENCES

- Abadi, M. G., Navarro, J. F., Steinmetz, M., Eke, V. R. 2003, *ApJ*, 597, 21
 Adibekyan, V. Z., Figueira, P., Santos, N. C., et al. 2013, *A&A*, 554, A44
 Amarante, J. A. S., Beraldo e Silva, L., Debattista, V. P., et al. 2020, *ApJL*, 891, L30
 Anders, G., Chiappini, C., Santiago, B. X., et al. 2014, *A&A*, 564, A115
 Antoja, T., Helmi, A., Dehnen, W., et al. 2014, *A&A*, 563, A60
 Aumer, M., White, S. D. M. 2013, *MNRAS*, 428, 1055
 Barbanis, B., Woltjer, L. 1967, *ApJ*, 150, 461
 Belokurov, V., Erkal, D., Evans, N. W., et al. 2018, *MNRAS*, 478, 611
 Bensby, T., Feltzing, S., Lundström, I., Ilyin, I. 2005, *A&A*, 433, 185
 Bensby, T., Zenn, A. R., Oey, M. S., et al. 2007, *ApJL*, 663, L13
 Bensby, T., Alves-Brito, A., Oey, M. S., Yong, D., Meléndez, J., 2011, *ApJL*, 735, L46
 Bensby, T., Feltzing, S., & Oey, M. S. 2014, *A&A*, 562, A71
 Bland-Hawthorn, J., Gerhard, O. 2016, *ARA&A*, 54, 529
 Bland-Hawthorn, J., Sharma, S., Tepper-García, T., et al. 2018, *MNRAS*, 486, 1167
 Boeche, C., Siebert, A., Piffl, T., et al. 2013, *A&A*, 559, A59
 Bournaud, F., Elmegreen, B. G., & Martig, M. 2009, *ApJ*, 707, L1
 Bovy, J., Rix, H.-W., & Hogg, D. W. 2012a, *ApJ*, 751, 131
 Bovy, J., Rix, H. W., Liu, C., et al. 2012b, *ApJ*, 753, 148
 Bovy, J., Nidever, D. L., Rix, H. W., et al. 2014, *ApJ*, 790, 127
 Bovy, J. 2015, *ApJS*, 216, 29
 Bovy, J., Rix, H. W., Schlafly, E. F., et al. 2016, *ApJ*, 823, 30
 Bilir, S., Karaali, S., Gilmore, G. 2006, *MNRAS*, 366, 1295
 Bilir, S., Karaali, S., Ak, S., et al. 2012, *MNRAS*, 421, 3362
 Bird, J. C., Loebman, S. R., Weinberg, D. H., et al. 2021, *MNRAS*, 503, 1815
 Bournaud, F., Elmegreen, B. G., & Elmegreen, D. M. 2007, *ApJ*, 670, 237
 Brook, C. B., Kawata, D., Gibson, B. K., & Freeman, K. C. 2004, *ApJ*, 612, 894
 Brook, C. B., Gibson, B. K., Martel, H., & Kawata, D. 2005, *ApJ*, 630, 298
 Brook, C., Richard, S., Kawata, D., Martel, H., & Gibson, B. K. 2007, *ApJ*, 658, 60
 Brook, C. B., Stinson, G. S., Gibson, B. K., et al. 2012, *MNRAS*, 426, 690
 Cannon, R. D. 1970, *MNRAS*, 150, 111
 Carrell, K., Chen, Y., Zhao, G. 2012, *AJ*, 144, 185
 Carrillo, I., Minchev, I., Steinmetz, M., et al. 2019, *MNRAS*, 490, 797
 Chang, C. K., Ko, C. M., Peng, T. H. 2011, *ApJ*, 740, 34
 Chen, Y. Q., Zhao, G., Carrell, K., Zhao, J. K. 2011, *AJ*, 142, 184
 Chiappini, C., Matteucci, F., & Gratton, R. 1997, *ApJ*, 477, 765
 Chiappini, C., Anders, F., Rodrigues, T. S., et al. 2015, *A&A*, 576, L12
 Clarke, A. J., Debattista, V. P., Nidever, D. L., et al. 2019, *MNRAS*, 484, 3476
 Coskunoğlu, B., Ak, S., Bilir, S., et al. 2012, *MNRAS*, 419, 2844
 Cui, X. Q., Zhao, Y. H., Chu, Y. Q., et al. 2012, *RAA*, 12, 1197
 Deason, A. J., Belokurov, V., Kopusov, S. E., et al. 2018, *ApJ*, 862, 1D
 Dehnen, W. 2000, *AJ*, 119, 800
 Deng, L. C., Newberg, H. J., Liu, C., et al. 2012, *RAA*, 12, 735
 Donor, J., Frinchaboy, P. M., Cunha, K., et al. 2020, *AJ*, 159, 199
 Du, C. H., Zhou, X., Ma, J., et al. 2003, *A&A*, 407, 541
 Du, C. H., Ma, J., Wu, Z. Y., Zhou, X. 2006, *MNRAS*, 372, 1304
 Fuhrmann, K. 1998, *A&A*, 338, 161
 Fuhrmann, K. 2008, *MNRAS*, 384, 173
 Gaia Collaboration, Katz, D., Antoja, T., Romero-Gómez, M., et al. 2018, *A&A*, 616, A11
 Gaia Collaboration, Creevey, O. L., Sarro, L. M., et al. 2023a, *A&A*, 674, A39
 Gaia Collaboration, Recio-Blanco, A., Kordopatis, G., et al. 2023b, *A&A*, 674, A38
 García Pérez, A. E., Allende Prieto, C., Holtzman, J. A., et al. 2016, *AJ*, 151, 144
 Gent, M. R., Eitner, P., Serenelli, A., et al. 2022, arXiv:2206.10949
 Gilmore, G., & Reid, N. 1983, *MNRAS*, 202, 1025
 Gómez, F. A., Minchev, I., Villalobos, A., O’Shea, B. W., & Williams, M. E. K. 2012a, *MNRAS*, 419, 2163

- Gómez, F. A., Minchev, I., O'Shea, B. W., et al. 2012b, *MNRAS*, 423, 3727
- Grand, R. J. J., Springel, V., Gómez, F. A., et al. 2016, *MNRAS*, 459, 199
- Guiglion, G., Recio-Blanco, A., de Laverny, P., et al. 2015, *A&A*, 583, A91
- Han, D. R., Lee, Y. S., Kim, Y. K., et al. 2020, *ApJ*, 896, 14H
- Hartkopf, W. I. & Yoss, K. M. 1982, *AJ*, 87, 1679
- Hayden, M. R., Bovy, J., Holtzman, J. A., et al. 2015, *ApJ*, 808, 132
- Hayden, M. R., Recio-Blanco, A., de Laverny, P., et al. 2017, *A&A*, 608, L1
- Hayden, M. R., Bland-Hawthorn, J., Sharma, S., et al., 2020, *MNRAS*, 493, 2952
- Haywood, M., Di Matteo, P., Lehnert, M. D., et al. 2013, *A&A*, 560, A109
- Hekker, S., & Johnson, J. A., 2019, *MNRAS*, 487, 4343
- Helmi, A., Babusiaux, C., Koppelman, H. H., et al. 2018, *Nature*, 563, 85
- Huang, Y., Liu X. W., Yuan H. B., et al., 2015, *MNRAS*, 449, 162
- Huang, Y., Liu, X. W., Yuan, H. B., et al., 2016, *MNRAS*, 463, 2623
- Huang, Y., Schönrich, R., Liu, X. W., et al., 2018, *ApJ*, 864, 129
- Huang, Y., Schönrich, R., Zhang, H. W., et al., 2020, *ApJS*, 249, 29
- Hunt, J. A. S., Bovy, J., Pérez-Villegas, A., et al. 2018, *MNRAS*, 474, 95
- Hunter, C., Toomre, A. 1969, *ApJ*, 155, 747
- Imig, J., Price, C., Holtzman, J. A., et al. 2023, *ApJ*, 954, 124
- Jenkins, A. 1992, *MNRAS*, 257, 620
- Jia, Y. P., Du, C. H., Wu, Z. Y., et al. 2014, *MNRAS*, 441, 503
- Jing, Y., Du, C., Gu, J., et al. 2016, *MNRAS*, 463, 3390
- Jofré, P., Jorissen, A., Van Eck, S., et al. 2016, *A&A*, 595, A60
- Jurić, M., Ivezić, Ž., Brooks, A., et al. 2008, *ApJ*, 673, 864
- Kalnajs, A. J. 1991, *Dynamics of Disc Galaxies*, 323
- Karaali, S., Bilir, S., Yaz, E., Hamzaoglu, E., Buser, R. 2007, *PASA*, 24, 208
- Katz, D., Soubiran, C., Cayrel, R., et al. 2011, *A&A*, 525, A90
- Katz, D., Gómez, A., Haywood, M., et al. 2021, *A&A*, 655, A111
- Kawata, D. & Chiappini, C. 2016, *Astronomische Nachrichten*, 337, 976
- Kawata, D., Grand, R. J. J., Gibson, B. K., et al. 2017, *MNRAS*, 464, 702
- Kazantzidis, S., Bullock, J. S., Zentner, A. R., et al. 2008, *ApJ*, 688, 254
- Khoperskov, S., Bertin, G. 2017, *A&A*, 597, A103
- Kordopatis, G., Recio-Blanco, A., de Laverny, P., et al. 2011, *A&A*, 535, 107
- Kordopatis, G., Binney, J., Gilmore, G., et al. 2015, *MNRAS*, 447, 3526
- Kordopatis, G., Wyse, R. F. G., Chiappini, C., et al. 2017, *MNRAS*, 467, 469
- Kruijssen, J. M. D., Pfeffer, J. L., Reina-Campos, M., et al. 2019, *MNRAS*, 486, 3180
- Laporte, C. F. P., Gómez, F. A., Besla, G., Johnston, K. V., & Garavito-Camargo, N. 2018, *MNRAS*, 473, 1218
- Lee, Y. S., Beers, T. C., An, D., et al. 2011, *ApJ*, 738, 187
- Li, C. D., Zhao, G. 2017, *ApJ*, 850, 25
- Li, C. D., Zhao, G., Zhai, M., Jia, Y. P. 2018, *ApJ*, 860, 53
- Li, X. Y., Huang, Y., Chen, B. Q., et al. 2020, *ApJ*, 901, 56
- Lian, J., Thomas, D., Maraston, C., et al. 2020, *MNRAS*, 494, 2561
- Lian, J., Zasowski, G., Havelquist, S., et al. 2022, *MNRAS*, 511, 5639
- Liu, X. W., Yuan, H. B., Huo, Z. Y., et al. 2014, in *IAU Symp. 298, Setting the Scene for Gaia and LAMOST* (Cambridge: Cambridge Univ. Press), 310
- Loebman, S. R., Roškar, R., Debattista, V. P., et al. 2011, *ApJ*, 737, 8
- Mackereth, J. T., Bovy, J., Schiavon, R. P., et al. 2017, *MNRAS*, 471, 3057
- Mackereth, J. T., Bovy, J., Leung, H. W., et al. 2019, *MNRAS*, 489, 176
- Majewski, S. R., Schiavon, R. P., Frinchaboy, P. M., et al. 2017, *AJ*, 154, 94
- Martig, M., Rix, H.-W., Silva Aguirre, V., et al. 2015, *MNRAS*, 451, 2230
- Matsuno, T., Yong, D., Aoki, W., et al. 2018, *ApJ*, 860, 49
- Minchev, I., Famaey, B. 2010, *ApJ*, 722, 112
- Minchev, I., Famaey, B., Quillen, A. C., et al. 2012, *A&A*, 548, A127
- Minchev, I., Chiappini, C., & Martig, M. 2013, *A&A*, 558, A9
- Minchev, I., Chiappini, C., Martig, M., et al. 2014, *ApJL*, 781, L20
- Minchev, I., Martig, M., Streich, D., et al. 2015, *ApJ*, 804, L9
- Miranda, M. S., Pilkington, K., Gibson, B. K., et al. 2016, *A&A*, 587, A10
- Momany, Y., Zaggia, S., Gilmore, G., et al. 2006, *A&A*, 451, 515
- Nidever, D. L., Bovy, J., Bird, J. C., et al. 2014, *ApJ*, 796, 38
- Paczyński, B., & Stanek, K. Z. 1998, *ApJL*, 494, L219
- Pilkington, K., Few, C. G., Gibson, B. K., et al. 2012, *A&A*, 540, A56
- Poggio, E., Drimmel, R., Lattanzi, M. G., et al. 2018, *MNRAS*, 481, L21
- Queiroz, A. B. A., Anders, F., Chiappini, C., et al. 2020, *A&A*, 638, A76
- Quinn, P. J., Hernquist, L., & Fullagar, D. P. 1993, *ApJ*, 403, 74
- Recio-Blanco, A., de Laverny, P., Kordopatis, G., et al. 2014, *A&A*, 567, A5
- Recio-Blanco, A., de Laverny, P., Palicio, P. A., et al. 2023, *A&A*, 674, A29
- Reid, M. J., & Brunthaler, A. 2004, *ApJ*, 616, 872
- Reid, M. J., Menten, K. M., Brunthaler, A., et al. 2014, *ApJ*, 783, 130
- Robin, A. C., Bienaymé, O., Salomon, J. B., et al. 2022, *A&A*, 667, A98
- Roškar, R., Debattista, V. P., Brooks, A. M., et al. 2010, *MNRAS*, 408, 783
- Roškar, R., Debattista, V. P., Quinn, T. R., & Wadsley, J. 2012, *MNRAS*, 426, 2089
- Sales, L. V., Helmi, A., Abadi, M. G., et al. 2009, *MNRAS*, 400, L61
- Sellwood, J. A., & Binney, J. J. 2002, *MNRAS*, 336, 785
- Schönrich, R., Binney, J. 2009, *MNRAS*, 399, 1145
- Schönrich, R., Binney, J., & Dehnen, W. 2010, *MNRAS*, 403, 1829
- Schönrich, R. 2012, *MNRAS*, 427, 274
- Schönrich, R., & McMillan, P. J. 2017, *MNRAS*, 467, 1154
- Schönrich, R., & Dehnen, W., 2018, *MNRAS*, 478, 3809
- Soubiran, C., Bienaymé, O., & Siebert, A. 2003, *A&A*, 398, 141
- Spagna, A., Lattanzi, M. G., Re Fiorentin, P., Smart, R. L. 2010, *A&A*, 510, L4
- Spina, L., Ting, Y. S., De Silva, G. M., et al. 2021, *MNRAS*, 503, 3279
- Spitoni, E., Silva Aguirre, V., Matteucci, F., et al. 2019, *A&A*, 623, A60
- Spitzer, L. J., Schwarzschild, M. 1951, *ApJ*, 114, 385
- Spitzer, L. J., Schwarzschild, M. 1953, *ApJ*, 118, 106
- Sun, W. X., Huang, Y., Wang, H. F., et al. 2020, *ApJ*, 903, 12
- Sun, W. X., Shen, H., & Liu, X. W. 2023, *ApJ*, 952, 163
- Sun, W. X., Huang, Y., Shen, H., et al. 2024, *ApJ*, 961, 141
- Tunçel, G. S., Bilir, S., Karaali, S., et al. 2019, *AdSpR*, 63, 1360
- Vickers, J. J., Shen, J. T., Li, Z. Y. 2021, *ApJ*, 922, 189
- Villalobos, Á., & Helmi, A. 2008, *MNRAS*, 391, 1806
- Wisnioski, E., Förster Schreiber, N. M., Wuyts, S., et al. 2015, *ApJ*, 799, 209
- Wyse, R. F. G., & Gilmore, G. 1995, *AJ*, 110, 2771
- Xiang, M. S., Liu, X. W., Yuan, H. B., et al. 2015, *MNRAS*, 448, 822
- Yan, Y., Du, C., Liu, S., et al. 2019, *ApJ*, 880, 36
- Yong, D., Carney, B. W., Friel, E. D. 2012, *AJ*, 144, 95
- Yong, D., Casagrande, L., Venn, K. A., et al. 2016, *MNRAS*, 459, 487
- Yoshii, Y. 1982, *PASJ*, 34, 365
- Yuan, H. B., Liu, X. W., Huo, Z. Y., et al. 2015, *MNRAS*, 448, 855
- Zhang, H. P., Chen, Y. Q., Zhao, G. 2021, *ApJ*, 919, 52